Review Article

Yanlong Han#, Haoyuan Lei#, Habaxi·Kaken, Wei Zhao, Wei Wang, Aikebaier·Wumanerjiang, Wei Peng, Likun Guo, Linxia Gu, Qingquan Kong, Changchun Zhou, and Li Wang*

3D printing customized design of human bone tissue implant and its application

https://doi.org/10.1515/ntrev-2022-0049
received October 6, 2021; accepted January 4, 2022

Abstract: Three-dimensional (3D) printing technology has the advantages of fast design and fabrication in clinical orthopedics. This study proposed the application of 3D-printed personalized reverse shoulder prosthesis in a reverse total shoulder arthroplasty for a patient with tuberculosis of the shoulder joint. Traditional and personalized shoulder prostheses were compared and studied. The mechanical simulation analysis was conducted on the individualized prosthesis and scapula. A personalized reverse total shoulder prosthesis was fabricated by 3D printing technology. Finite element analyses were conducted for implantation of traditional and personalized prostheses. The numerical results show that the maximum equivalent stress of screws inserted into bone tissue is 43.23 MPa in the personalized prosthesis. But in traditional prostheses, the maximum equivalent stress of screws performing the same function is 246.50 MPa. The structural advantages of the personalized prosthesis effectively reduce the local pressure of the screws to ensure the safety and effectiveness of the material during service. At the same time, the scapula paired with the personalized prosthesis also shown a smaller mean equivalent stress that can reduce patient stress. The postoperative evaluation of implant stability and patient status was good. The results indicated that 3D printing technology has important application value in orthopedic surgery.

Keywords: 3D printing, bone tissue implant, personalized design, finite element analysis

1 Introduction

Bone tuberculosis (TB) is a destructive disease caused by the invasion of bone or joints by *Mycobacterium tuberculosis*, which is generally divided into two types of articular and spinal TB. The location of the formation of articular TB includes the hip, knee, foot, elbow, *etc*., among which TB of the shoulder joint is a rare disease with an incidence of only 0.9–1.7%, and it is difficult to cure [1]. There is no standard treatment plan for TB of the shoulder joint at present. Traditional treatment methods include surgery and anti-TB drug therapy [2]. However, in some specific serious cases, joint transplantation or shoulder replacement implants are required to reconstruct shoulder function. Especially, for the end-stage shoulder diseases, the treatment of artificial shoulder replacement is quite challenge for clinician [3]. The shoulder joint has a complex anatomical structure, which is very difficult to operate in the replacement process. Unsuitable implants are at a high risk of instability and dislocation. It may lead to joint infections, loosening of the prosthesis, and fractures in adjacent bones [4–7].

Three-dimensional (3D) printing is a type of rapid prototyping technology, also known as additive manufacturing, which builds 3D entities by stacking printable materials layer by layer based on computer digital models.

# These authors contributed equally to this work.

*** Corresponding author: Li Wang,** Department of Orthopedics, The People's Hospital of Xinjiang Uygur Autonomous Region, Urumqi 830001, China, e-mail: doctorwanglixj@126.com
Yanlong Han, Habaxi·Kaken, Wei Zhao, Wei Wang, Aikebaier·Wumanerjiang: Department of Orthopedics, The People's Hospital of Xinjiang Uygur Autonomous Region, Urumqi 830001, China
Haoyuan Lei, Likun Guo, Changchun Zhou: College of Biomedical Engineering, Sichuan University, Chengdu 610064, China; National Engineering Research Center for Biomaterials, Sichuan University, Chengdu 610064, China
Wei Peng: Department of Palliative Care, West China School of Public Health and West China Fourth Hospital, Sichuan University, Chengdu, 610041, China
Linxia Gu: Department of Biomedical and Chemical Engineering and Sciences, College of Engineering & Science, Florida Institute of Technology, Melbourne, FL 32901-6975, United States of America
Qingquan Kong: Department of Orthopedics, West China Hospital, Sichuan University, Chengdu, 610041, China

In recent years, with the rapid development of 3D printing technology, the shapes of implant can be personalized design according to the characteristics of the patient's disease data and match the bone tissue defect of the host. 3D printing provides a new solution for the orthopedic implantation and artificial prosthesis [8–11]. Personalized design of human bone tissue implant based on 3D printing technology is conducive to rapid diagnosis and treatment of bone diseases [12,13]. In some special orthopedic diseases, the conventional standardized products cannot meet the clinical needs and need to customize the personalized tissue repair implants to treat. Traditional equal-material manufacturing and subtractive manufacturing are suitable for small batch processing of simple components, but difficult to produce complex medical implant devices with high precision requirements. In contrast, 3D printing can produce high-precision, high-quality complex shape parts, shorten the manufacturing cycle, save materials, and reduce costs, especially for the preparation of medical implants with precision requirements. In addition, titanium alloy has become the main choice for orthopedic implant materials because of its excellent mechanical and biological properties [14–17], such as high strength, good corrosion resistance, good heat resistance, and good biocompatibility. Titanium implants are usually fabricated by selective laser melting (SLM) 3D printing technology. SLM is a main technique in additive manufacturing of metal materials. This technology uses laser as the energy source and scans the metal powder bed layer by layer according to the path set in the 3D CAD slice model, so as to melt and solidify the metal powder and finally form a complete 3D entity. In this study, the titanium alloy artificial shoulder prosthesis was customized design based on the SLM technology, and the structure of traditional prosthesis was innovatively improved. The finite element analysis technology was used to simulate the force of both prostheses after implantation, and it was confirmed that the mechanical properties of the customized prosthesis were optimized compared with the traditional prosthesis, and it could play a better role in mechanical support and damage repair. Similar scientific research usually simulates the local stress distribution after shoulder prosthesis implantation through finite element analysis, and its research generally focuses on the influence of the fine-tuning of prosthesis structure or implantation mode on the simulation results. However, this fine-tuning, such as screw size and angle, basically does not change the gross structure of the prosthesis and is only applicable to the general situation of total shoulder joint replacement surgery. When facing patients with special symptoms such as large bone defects, the traditional prosthesis is no longer suitable. It is necessary to redesign the prosthesis structure according to the characteristics of disease lesions and evaluate its theoretical effectiveness through simulation analysis, which is the innovation of this research.

2 Materials and methods

2.1 Customized requirements for shoulder joint prosthesis design

The requirements for personalized customization of shoulder prosthesis come from the clinical diagnosis of this patient. Imaging and pathological examinations were performed on the patient.

Imaging findings revealed a thickened acromion and the wall of the slip capsule of patient's left shoulder joint. The smoothness of the articular surface appeared reduced, accompanied with narrow articular space. Uneven and obvious enhancement was appeared around persistent central necrosis in the posterior lower soft tissue of shoulder joint. Pathological findings showed coagulation necrosis of her left cervical lymph node, accompanied by epithelioid granulomatous inflammation and multinucleated giant cell reaction. Further tests were positive for TB.

Based on the above results, the patient was professionally diagnosed as shoulder TB with extensive osteonecrosis. Therefore, the patient needs to have the necrotic bone removed and shoulder replacement surgery performed. Therefore, a personalized shoulder prosthesis is required.

2.2 Design of personalized 3D prosthesis

Mimics19.0 was used to read the DICOM data obtained from computed tomographic (CT) detection of the patient, and the threshold range for hard bone segmentation was determined so as to reconstruct the left shoulder joint model of the patient. Based on the analysis of the reconstructed model, together with X-ray and magnetic resonance imaging results, the model is imported into 3-matic for personalized prosthesis design [18]. Based on the existing research reports and clinical application cases, the traditional shoulder prosthesis structure was optimized according to the specific disease characteristics of

the patient; a new type of shoulder joint prosthesis model was established.

2.3 3D printing of personalized shoulder joint

The prosthesis model was imported into Materialise Magics 22.0 for slice layerization to export the data information and printing path of each layer which were determined. The titanium alloy prosthesis was fabricated by laser selective melting technique with a commercial SLM machine (MLab cusing R, CONCEPTLASER, Germany). The raw material is medical-grade Ti6Al4V powder with particle size of 15–45 μm. The printer uses a laser system with a wavelength of 1,070 nm and a focusing beam region with a diameter of 50 μm. According to the data information of the current layer of the model, laser beam is used to selectively melt the powder on the substrate so as to form the shape of the current layer of the part. The complete solid part was manufactured by melting and solidification of the powders layer by layer [19]. During printing, the parameters are set with laser power of 100 W, scanning speed of 900 mm/min, scanning interval of 110 μm, and monolayer powder thickness of 25 μm [20], and the orthogonal scanning path and contoured thermal support are adopted. The whole printing process is protected by high purity argon gas, and the oxygen content in the working space is below 0.5%. After removing the support and heat treatment, the dimension accuracy error of the 3D-printed personalized shoulder joint prosthesis is less than 1%.

3 Results and discussions

3.1 Design of personalized 3D-printed prosthesis

Prosthesis and scapula models were designed based on the CT data of the patient. As shown in Figure 1(a). The hemispherical structure is an imitation of the patient's massive necrosis and humeral head defect. The gradient base pad enlarges the contact surface, increases the initial stability, and preserves the glenoid bone substance to a certain extent. The multi-screw structure with an outward inclined angle increases the depth, fixation range,

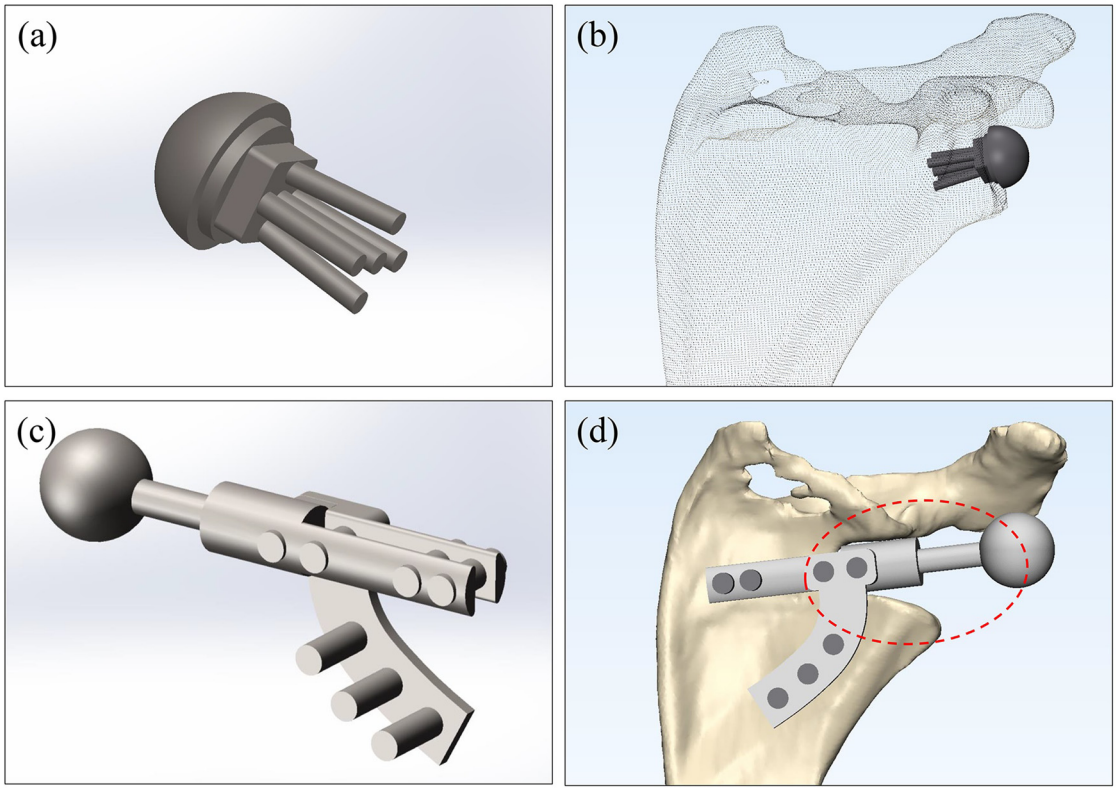

Figure 1: Prosthesis and scapula models: (a) the model of traditional reverse shoulder joint prosthesis that faces the glenoid; (b) the model of scapula with implanted traditional prosthesis; (c) the model of personalized reverse shoulder joint prosthesis that faces the shoulder joint; (d) the model of scapula with implanted personalized prosthesis.

and stability of the implant. The traditional prosthesis is suitable for shoulder joint replacement in which the components of the scapula are complete and the glenoid can bear force normally. The prosthesis is inserted into the glenoid with screws and immediate stability was achieved; Figure 1(b) shows how it matches with the scapula. Nevertheless, the patient had a special lesion location. Due to the partially necrotic and defective scapula, fragile glenoid, and incapable of bearing strength, it was infeasible for shoulder joint replacement due to the loss of the effective fit structure of traditional prosthesis implantation.

In view of the above reasons, a reverse shoulder joint prosthesis is customized for the patient, as shown in Figure 1(c). From the reconstructed model of patient's lesion, it can be found that the humeral head is flat, collapsed, and necrotic, much bone tissue had lost in the affected area, and the glenoid is severely damaged under the long-term impact of TB of shoulder joint. To ensure the normal function of the scapula after surgery, the original residual bone tissue structure in the red-dashed ellipse in Figure 1(d) needs to be removed. Because the bone including the entire glenoid has been removed, the traditional prosthesis is no longer applicable. Instead, a personalized prosthesis that can replace the removed bone tissue structure is designed. This personalized prosthesis replaces the traditional hemispherical structure with a spherical structure that better mimics the humerus head, providing greater flexibility and a smoother connection to the prosthetic link rod. With the aid of the main prosthesis and the auxiliary curved handle, it is fixed on a larger surface of the scapula in a Y shape through screws inserted into the bone tissue, as shown in Figure 1(d). By fixing the prosthesis on a larger area of the scapula, the stress on the scapular is not concentrated near the glenoid, so that the pressure of the screws is distributed to the entire scapula and the main body of the prosthesis. It is intended to enhance the long-term stability of the structure and function of the prosthesis after implantation and reduce the stress on the scapula. At the same time, to achieve the flexibility of the joint, the size of the personalized prosthesis was determined by referring to the size parameters of the traditional prosthesis and the structural characteristics of patient's shoulder blade. For example, the spherical structure of the prosthesis is similar in size to the humeral head, and the clavicular structure is similar in thickness to the corresponding part of the scapula. Therefore, the personalized prosthesis fits tightly with the shoulder blade, realizing the shape replacement and function remodeling and ensuring the joint flexibility.

3.2 Mechanical properties simulation of personalized prosthesis

To verify the mechanical properties of the personalized prosthesis, the finite element method is used for simulation analysis. The established structural models of prosthesis and scapula are input into the ABAQUS. These models have been meshed and exported in 3-matic in advance [21,22]. The quality of meshing plays a pivotal role in the calculation time and simulation accuracy. We adopted the uniform remesh with high quality and divided the prosthesis and scapula with different material attributes into different sizes of mesh according to the calculation accuracy requirements, as shown in Figure 2. The traditional prosthesis was divided into 277,266 meshes with a side length of 0.125 mm, and the corresponding scapula was divided into 307,278 meshes with a side length of 0.5 mm. The personalized prosthesis was divided into 481,148 meshes with a side length of 0.25 mm, and the corresponding shoulder blades were divided into 249,704 meshes with a side length of 0.5 mm. It can be seen that the grids are closely distributed in structure, orderly arranged, and consistent in size. The ratio of height to width of the nontwisted grid is similar. Moreover, the transition of the grids at the corners of the structure is natural, and there is no grid distortion. Overall, the grids are well divided. Specifically, Figure 2(a–c) shows the grids of the personalized prosthesis and scapula matching model and the corresponding enlarged views. Figure 2(d–f) shows the grid chart of the traditional prosthesis and scapula matching model and the corresponding enlarged views.

Different material properties are assigned to the prosthesis and the scapula. The medical titanium alloy Ti6Al4V, which is used as the raw material for manufacturing clinical implants, is a material conforming to Von Mises yield criterion. By referring to relevant research and the standard manual [23–29], the parameters of Ti6Al4V are determined and assigned to the prosthesis model, with ultimate yield strength of 1,000 MPa, density of 4,420 kg/m^3, Young's modulus of 109 GPa, and Poisson's ratio of 0.31. Similarly, according to the medical definition of human bones and the standard database, cortical bone parameters are assigned to the scapula, with ultimate yield strength of 100 MPa, density of 1,700 kg/m^3, Young's modulus of 13.8 GPa, and Poisson's ratio of 0.35.

To verify the accuracy of the simulation results, the analysis steps are implicitly created, and the stiffness matrix is solved iteratively to make the formula converge. When establishing boundary conditions and interactions,

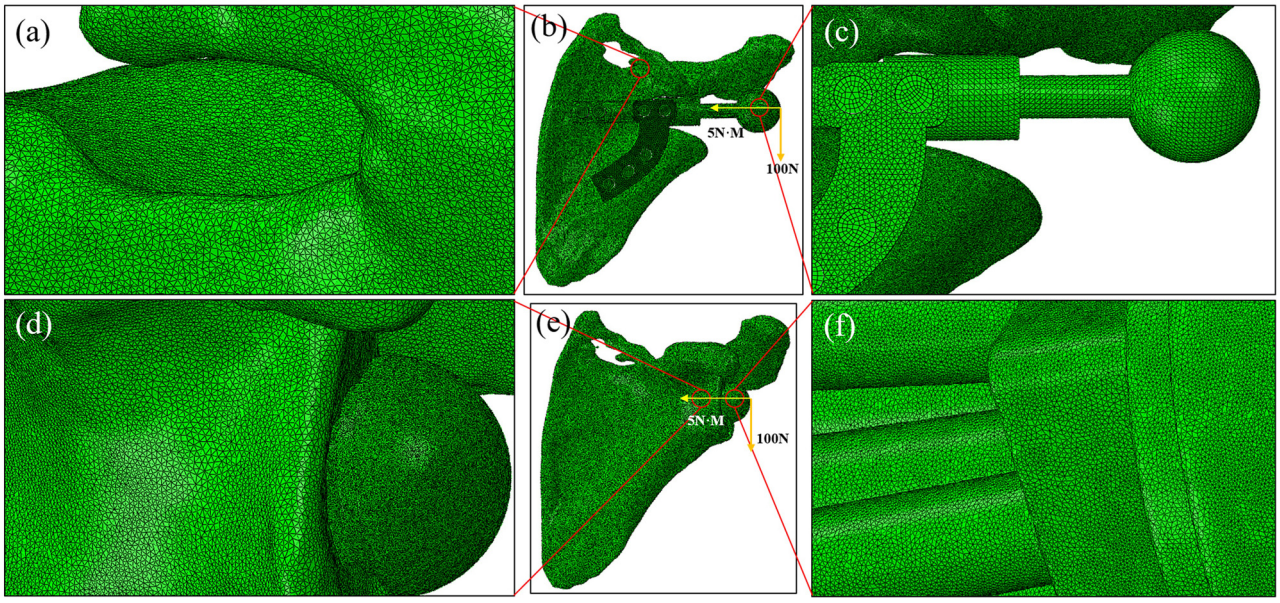

Figure 2: Mesh division and load application before finite element analysis. (a–c) Mesh chart of the personalized prosthesis and scapula matching model and the corresponding enlarged views. (d–f) Mesh chart of the traditional prosthesis and scapula matching model and the corresponding enlarged views.

first add constraint relationships to bind the screws inserted into the prosthesis and the corresponding screw holes on the scapula, and then couple the sphere structure of the prosthesis to a reference point on the sphere. Subsequently, a load vector of 100 N and a bending moment of 5 N M are added on the determined reference point to simulate the stress on the human shoulder joint movement. The force directions are shown in Figure 2(a) and (b). This reference point is coupled to the sphere model, and the load uniformly distributed on the sphere structure is equivalent to the force acting on the reference point. The Von Mises equivalent stress is selected as the cloud chart index to analyze the stress distribution of the contacting part of the prosthesis and the scapula, so as to investigate the simulated mechanical properties and the degree of fit of the prosthesis.

3.3 Comparative analysis of the mechanical properties between personalized and conventional prosthesis

Figure 3 shows the cloud diagrams of the Von Mises equivalent stress distribution of the traditional prosthesis and the scapula. In the color distribution legend in the upper left corner, the stress gradually increases from blue at the bottom to red at the top, covering the stress value range from 0 to the maximum of the results. As can be seen from Figure 3(a), the larger stresses are mainly distributed at the contact parts between the inserted screws and the glenoid. After traditional prosthesis implantation, the maximum equivalent stress of scapula does not excess 46.43 MPa, while the equivalent stress of the part not directly contacting the prosthesis is not more than 30.95 MPa, both were less than the ultimate yield strength of cortical bone (about 100.00 MPa), as shown in Figure 3(b). The larger stresses on the implanted prosthesis are concentrated near the screws, among which the maximum is 246.5 MPa, at the insertion interface of the screw and the glenoid. The stress on the rest part of the prosthesis is smaller, below the ultimate yield strength (about 1000.00 MPa) of Ti6Al4V, as shown in Figure 3(c) and (d).

Overall, the simulation shows that the conventional reverse shoulder joint prosthesis is in good state of stress, with the stress range being less than the threshold range. However, as mentioned above, the patient in this case has a complex condition. It is difficult for the severely damaged glenoid to bear force, so the traditional prosthesis cannot be inserted directly. Instead, the damaged bone tissue around the glenoid needs to be removed, so there exists necessity to design a personalized prosthesis to replace the structure and function of the removed bone tissue. At the same time, it is observed that although the stress ranges within the thresholds, the large stresses on

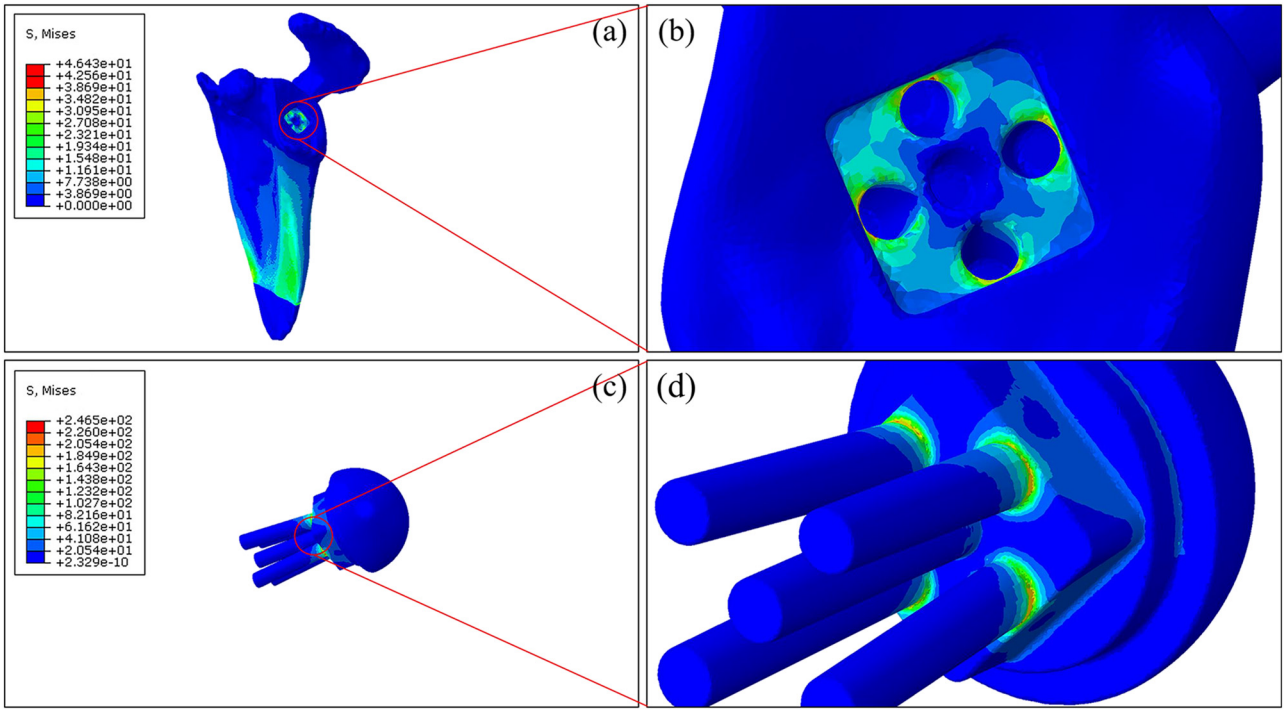

Figure 3: Finite element analysis results after implantation of traditional prosthesis. (a) Stress cloud diagram of the scapula after implantation of traditional prosthesis; (b) enlarged view of glenoid; (c) stress cloud diagram of the implanted traditional prosthesis; and (d) enlarged view of screw interface.

the scapula are mostly concentrated at the joint of the glenoid corresponding to the inserted screws. Long-term stress may lead to bone resorption and internal low-density cancellous bone wear, the loosening, displacement, and detaching of the implanted metal prosthesis, joint infection and instability, systemic fractures, sports injuries, and postoperative pain. This significantly reduces the patient's quality of life and can lead to a second operation and more serious consequences.

Simulation analysis of personalized prosthesis is performed under the same conditions. With the material properties, analysis step parameters and resolver unchanged, the interaction between personalized prosthesis and corresponding shoulder joint was constructed with the same definition. The screws inserted into the implanted prosthesis are bound with the corresponding screw holes on the scapula, and the same load vector is applied to simulate the situation of the personalized prosthesis model after implantation. Figure 4 shows the Von Mises equivalent stress distribution cloud diagram of the personalized prosthesis and the scapula.

As shown in Figure 4(a), by comparing the model surface with the colors in the stress distribution table at the upper left corner of the picture, it can be found that most of the equivalent stresses of the scapula are below 15.23 MPa, lower than the ultimate yield strength (about 100.00 MPa) of the cortical bone. The average equivalent stress on the scapula in the personalized prosthesis case is smaller than that in the traditional prosthesis case, with better simulation results. Additionally, the large stress in the red dashed circle in Figure 4(b) is a defect on the grid caused by single-point distortion, and its numerical result is wrong, which cannot reflect the real stress and has no reference value.

When analyzing the equivalent stress of the personalized prosthesis, the screw structure is separated from the main body of the prosthesis. It can be observed from Figure 4(c) that most of the large stresses are concentrated at the connecting rod, the stress on which is directly related to the length and diameter of the rod. The maximum stress is 118.70 MPa, much smaller than the ultimate yield strength (about 1000.00 MPa) of Ti6Al4V. The equivalent stress on the rod is proportional to the length of the rod and inversely proportional to the diameter of the rod, which is similar to the principle of leverage. However, in this research, we do not make too much analysis on the force of the rod. Although the equivalent stress of the rod is relatively large, it is far less than the ultimate yield strength of the material, and it has almost no influence on the stability of the

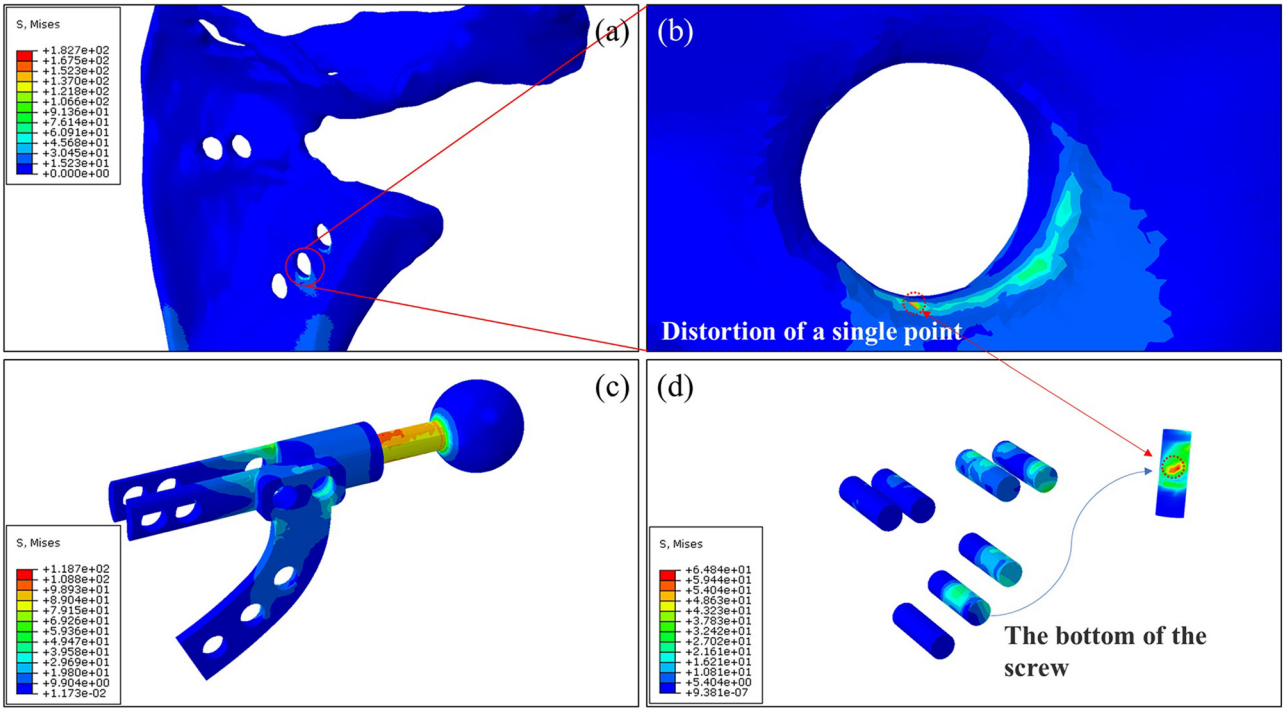

Figure 4: Finite element analysis results after implantation of personalized prosthesis: (a) stress cloud diagram of the scapula after implantation of personalized prosthesis; (b) enlarged view of a screw hole; (c) stress cloud diagram of the implanted personalized prosthesis; and (d) stress cloud diagram of screws.

prosthetic and scapula fit, so it is not the focus of consideration. By contrast, the equivalent stress of the screw is smaller, as shown in Figure 4(d). Except for the excessive stress induced by the distortion point, the equivalent stress is on the whole not higher than 43.23 MPa. Compared with the maximum stress of 246.50 MPa on the interface of screw in traditional prosthesis, the stress on the screw after implantation of the personalized prosthesis is significantly reduced.

Regardless of the influence of single-point distortion, the simulated equivalent stress analysis results of traditional prosthesis and personalized prosthesis are compared, and a histogram is drawn to be shown in Figure 5. In order to better show the force of each part, the scapula, prosthesis (without screws), and screws are analyzed separately. It can be observed that the maximum equivalent stresses of scapula after implantation of traditional and personalized prostheses are close, without significant differences. However, according to the analysis in the previous part of this study, the average equivalent stress of scapula matched with personalized prosthesis is smaller and more evenly distributed. The main body of traditional prosthesis bears small forces, with a maximum of 61.62 MPa, yet the bearing strengths of screws are

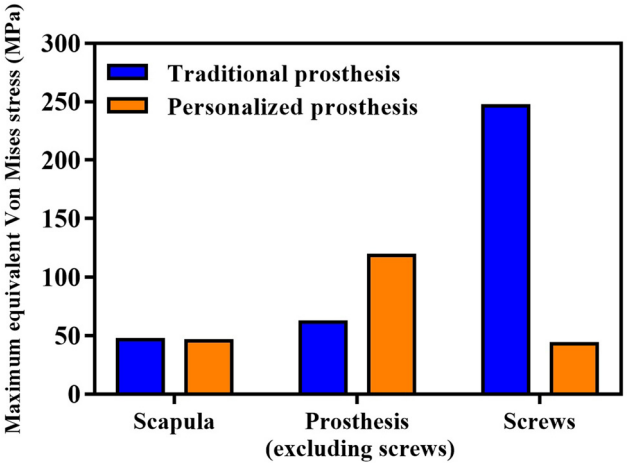

Figure 5: Histograms of the maximum equivalent Von Mises stress of the two prostheses and the corresponding scapulae under the same load.

large, with a maximum of 246.50 MPa. For the personalized prosthesis, stress on the connecting rod is larger, with a maximum of 118.70 MPa, while the screws bear smaller forces, with a maximum of 43.23 MPa.

The screws which are implanted or inserted into the bone will directly contact the bone after implantation,

and the stress on the screws directly affects the repair performance of the implant and the patient's postoperative rehabilitation. Therefore, the equivalent stress of the screw is an important indicator to evaluate the mechanical properties of the prosthesis. By optimizing the structural design of the personalized prosthesis, the screws were dispersed on the main body of the prosthesis. Compared with the traditional prosthesis, the equivalent stress of the personalized prosthesis body is increased within the acceptable range, while the screw equivalent stress is significantly reduced, which greatly relieves the screw pressure. At the same time, the personalized prosthesis reduces the burden on the scapula as well as the risks of wear and resorption of low-density cancellous bone due to long-term stress after implantation. It also decreases the risks of displacement and detachment of implanted metal prosthesis, joint infection and instability, postoperative pain, systemic fracture, and a second operation.

3.4 Evaluation of surgical efficacy and functions

The personalized customized 3D-printed shoulder prosthesis was highly consistent with the bone defects. After implantation, the soft tissues around the shoulder joint were successfully sewn into the prosthesis. The X-ray image done one day postoperative already showed that the prosthesis was in accurate position (Figure 6(a)). After 3 months' implantation, the postoperative X-ray result showed that the position of the prosthesis was still accurate (Figure 6(b)). The surgical incision healed well, and no postoperative complications were observed after surgery, including infection, fat liquefaction, and other postoperative complications. As shown in Figure 6(c) and (d), the range of motion (ROM) of the shoulder joint was checked at 7 and 15 months postoperatively and met the requirements of flexible movement. The whole arm was able to do activities of daily living easily, such as eating,

Figure 6: (a) The first day of postoperative X-ray showed that the position of the prosthesis was in accurate position; (b) the 3rd month of postoperative X-ray showed that the position of the prosthesis was accurate; (c) at the 7th month, the ROM of shoulder joint indicated that it was well restored; (d) at the 15th month, the ROM of shoulder joint indicated that it was well restored.

writing, driving, combing hair, and regular exercise. The function of shoulder joint was gradually well restored, and the quality of daily life was significantly improved. These results indicated that the reconstruction of shoulder joint function is successful, and the application of personalized shoulder joint prosthesis is effective.

4 Conclusion

The personalized shoulder joint prosthesis not only meets the special dimension requirements according patients, but also achieves ideal mechanical performance than that of traditional prosthesis. The personalized prostheses with high dimensional accuracy structure can effectively distribute the local high stress at the screws to the whole prosthesis trunk and can effectively distribute the stress concentrated at the glenoid to the whole scapula, which can reduce the risk of loosening after implantation and increase the service life of prostheses. At the same time, it can effectively meet some requirements of joint ROM while reduce postoperative risks and complications to ensure the quality of life of patients after surgery. Therefore, the combination of 3D printing technology and finite element analysis technology provides a robust solution for the clinical orthopedic repair.

Funding information: This work was partially supported by the National Key Research and Development Program of China (No. 2018YFC1106800, 2019YFA0110600). National Natural Science Foundation of China (31971251, 81871574). Science and Technology Project of Tibet Autonomous Region (XZ201901-GB-08), and the 1·3·5 Project for Disciplines of Excellence, West China Hospital, Sichuan University (ZYJC21026, ZYGD21001, ZYJC21077).

Author contributions: Y.H., C.Z., Q.K., L.G., and L.W. designed the project; H.L., H.K, W.Z., W.W., A.W., W.W., and L.G. collected data and prepared the figures; Y.H., H.L., and C.Z. wrote the main manuscript. All authors have accepted responsibility for the entire content of this study and approved its submission.

Conflict of interest: The authors state no conflict of interest.

Ethical approval: This study passed the ethical approval. Informed consent has been obtained from the patient for publication of the case details and images before this study. This study has been approved by the Ethics Committee of the People's Hospital of Xinjiang Uygur Autonomous Region. All methods were performed in accordance with the clinical trial guidelines and regulations.

References

[1] Sankaran B. Tuberculosis of bones & joints. Ind J Tub. 1993;40:109.
[2] Tang X, Guo W, Yang R, Tang S, Ji T. Synthetic mesh improves shoulder function after intraarticular resection and prosthetic replacement of proximal humerus. Clin Orthop Relat Res. 2015;473(4):1464–71.
[3] Werner BC, Burrus MT, Begho I, Gwathmey FW, Brockmeier SF. Early revision within 1 year after shoulder arthroplasty: patient factors and etiology. J Shoulder Elb Surg. 2015;24(12):E323–30.
[4] Linberg CJ, Sperling JW, Schleck CD, Cofield RH. Shoulder arthroplasty in morbidly obese patients. J Shoulder Elb Surg. 2009;18(6):903–6.
[5] Farng E, Zingmond D, Krenek L, SooHoo NF. Factors predicting complication rates after primary shoulder arthroplasty. J Shoulder Elb Surg. 2011;20(4):557–63.
[6] Singh JA, Sperling JW, Cofield RH. Revision surgery following total shoulder arthroplasty analysis of 2588 shoulders over three decades (1976 to 2008). J Bone Jt Surg Br. 2011;93b(11):1513–7.
[7] Rasmussen JV, Polk A, Brorson S, Sorensen AK, Olsen BS. Patient-reported outcome and risk of revision after shoulder replacement for osteoarthritis 1,209 cases from the Danish Shoulder Arthroplasty Registry, 2006–2010. Acta Orthop. 2014;85(2):117–22.
[8] Zhu YZ, Joralmon D, Shan WT, Chen YY, Rong JH, Zhao HY, et al. 3D printing biomimetic materials and structures for biomedical applications. Bio-Design Manuf. 2021;4(2):405–28.
[9] Tan HT, Yang KQ, Wei PG, Zhang GD, Dimitriou D, Xu L, et al. A novel preoperative planning technique using a combination of ct angiography and three-dimensional printing for complex toe-to-hand reconstruction. J Reconstr Microsurg. 2015;31(5):369–77.
[10] Wang D, Wang YM, Wang JH, Song CH, Yang YQ, Zhang ZM, et al. Design and fabrication of a precision template for spine surgery using selective laser melting (SLM). Materials. 2016;9(7):608.
[11] Oladapo BI, Zahedi SA, Ismail SO, Omigbodun FT, Bowoto OK, Olawumi MA, et al. 3D printing of PEEK-cHAp scaffold for medical bone implant. Bio-Design Manuf. 2021;4(1):44–59.
[12] Zhang B, Pei X, Zhou C, Fan Y, Jiang Q, Ronca A, et al. The biomimetic design and 3D printing of customized mechanical properties porous Ti6Al4V scaffold for load-bearing bone reconstruction. Mater Des. 2018;152:30–9.
[13] Zhang B, Sun H, Wu L, Ma L, Xing F, Kong Q, et al. 3D printing of calcium phosphate bioceramic with tailored biodegradation rate for skull bone tissue reconstruction. Bio-Design Manuf. 2019;2(3):161–71.
[14] Lei H, Yi T, Fan H, Pei X, Wu L, Xing F, et al. Customized additive manufacturing of porous Ti6Al4V scaffold with

micro-topological structures to regulate cell behavior in bone tissue engineering. Mater Sci Eng C Mater Biol Appl. 2021;120:111789.
[15] Song P, Hu C, Pei X, Sun J, Sun H, Wu L, et al. Dual modulation of crystallinity and macro-/microstructures of 3D printed porous titanium implants to enhance stability and osseointegration. J Mater Chem B. 2019;7(17):2865–77.
[16] Sun H, Hu C, Zhou CC, Wu LN, Sun JX, Zhou XD, et al. 3D printing of calcium phosphate scaffolds with controlled release o antibacterial functions for jaw bone repair. Mater Des. 2020;189:108540.
[17] Zhang LL, Zheng TT, Wu LL, Han Q, Chen SY, Kong Y, et al. Fabrication and characterization of 3D-printed gellan gum/starch composite scaffold for Schwann cells growth. Nanotechnol Rev. 2021;10(1):50–61.
[18] Baptista R, Pereira MFC, Mauricio A, Rechena D, Infante V, Guedes M. Experimental and numerical characterization of 3D-printed scaffolds under monotonic compression with the aid of micro-CT volume reconstruction. Bio-Design Manuf. 2021;4(2):222–42.
[19] Zhou C, Wang K, Sun Y, Wang Q, Jiang Q, Liang J, et al. Biofabrication (3D Bioprinting) Laboratory at Sichuan University. Bio-Design Manuf. 2021;4(2):432–9.
[20] Pei X, Wu L, Zhou C, Fan H, Gou M, Li Z, et al. 3D printed titanium scaffolds with homogeneous diamond-like structures mimicking that of the osteocyte microenvironment and its bone regeneration study. Biofabrication. 2021;13:015008.
[21] Pei X, Zhang B, Fan Y, Zhu X, Sun Y, Wang Q, et al. Bionic mechanical design of titanium bone tissue implants and 3D printing manufacture. Mater Lett. 2017;208:133–7.
[22] Allred JJ, Flores-Hernandez C, Hoenecke Jr HR, D'Lima DD. Posterior augmented glenoid implants require less bone removal and generate lower stresses: a finite element analysis. J Shoulder Elb Surg. 2016;25(5):823–30.
[23] Yu TY, Guo WF, Wang XJ, Liu JY, Wang Y, Chen MJ. Surface hydrophobicity and oleophilicity of hierarchical metal structures fabricated using ink-based selective laser melting of micro/nanoparticles. Nanotechnol Rev. 2020;9(1):626–36.
[24] Johnson JE, Caceres AP, Anderson DD, Patterson BM. Postimpingement instability following reverse shoulder arthroplasty: a parametric finite element analysis. Sem Arthroplasty JSES. 2021;31(1):36–44.
[25] Sabesan VJ, Lima DJL, Yang Y, Stankard MC, Drummond M, Liou WW. The role of greater tuberosity healing in reverse shoulder arthroplasty: a finite element analysis. J Shoulder Elb Surg. 2020;29(2):347–54.
[26] Virani NA, Harman M, Li K, Levy J, Pupello DR, Frankle MA. In vitro and finite element analysis of glenoid bone/baseplate interaction in the reverse shoulder design. J Shoulder Elb Surg. 2008;17(3):509–21.
[27] Yang CC, Lu CL, Wu CH, Wu JJ, Huang TL, Chen R, et al. Stress analysis of glenoid component in design of reverse shoulder prosthesis using finite element method. J Shoulder Elb Surg. 2013;22(7):932–9.
[28] Zhang M, Junaid S, Gregory T, Hansen U, Cheng CK. Impact of scapular notching on glenoid fixation in reverse total shoulder arthroplasty: an in vitro and finite element study. J Shoulder Elb Surg. 2020;29(10):1981–91.
[29] Carter DR, Hayes WC. The compressive behavior of bone as a two-phase porous structure. J Bone Jt Surg. 1977;59(7):954–62.